Investigation of the influence of the initial groove angle in the M-K model on limit strains and forming limit curves

Jie Ding[1], Cunsheng Zhang[1*], Xingrong Chu[2], Guoqun Zhao[1], Lionel Leotoing[3], Dominique Guines[3]

[1] Key Laboratory for Liquid-Solid Structural Evolution & Processing of Materials (Ministry of Education), Shandong University, Jinan 250061, P.R.China

[2] School of Mechanical, Electrical and Information Engineering, Shandong University, Weihai 264209, P.R.China

[3] Université Européenne de Bretagne, France, INSA-LGCGM - EA 3913 20, Avenue des Buttes de Coësmes 35043 RENNES Cédex

[*] Corresponding author. Tel.: +86(0)53181696555

E-mail address: zhangcs@sdu.edu.cn

Abstract

Marciniak-Kuczynski (M-K) model is the widely used method to theoretically obtain the forming limit curves (FLCs) of the sheet metal. However, in the applications of the M-K model, FLCs are generally assumed not to be dependent on the initial groove angle of the model, and are achieved with a zero groove angle. Nowadays, under positive strain paths, there is little research about whether the initial groove angle has influence on the limit strains and what the influence is. In addition, during the deduction of the M-K algorithm, the material's constitutive models with simple expressions are generally used, which cannot describe accurately the interacting effects of temperature and strain rate on forming limits. Therefore, above limitations greatly affect the accuracy of the predicted forming limits. In this work, three modified complex constitutive models

(Voce, Ludwik and Khan-Huang-Liang model), considering the interacting effects of temperature and strain rate, are implemented into M-K model to investigate the sheet formability of AA5086 under different temperatures (20, 150 and 200℃) and strain rates (0.02, 0.2 and 2s^{-1}). With the algorithm developed in this work, the influences of the initial groove angle on limit strains and FLCs are investigated. Results show that the initial groove angle has distinguishing influences on limit strains under different strain paths. When the strain path is in the range from 0 to 0.4, forming limits are always achieved with a zero groove angle. While when the strain path is not in the range from 0 to 0.4, limit strains depend greatly on the initial groove angle. The limit strains obtained with a zero groove angle in the literatures overestimate clearly its true sheet formability. Finally, the calculated limit strains are compared with experimental data obtained by Marciniak test under different forming conditions. Therefore, this work could provide an effective method to obtain the sheet formability more accurately by the M-K model.

Keywords：Marciniak-Kuczynski (M-K) model; Marciniak test; Initial groove angle; Forming limit curves (FLCs)

Notations

Ψ_0	Initial groove angle in the M-K model
Ψ	Current groove angle in the M-K model
$\Delta\Psi$	Groove angle increment
e_0^a, e_0^b	Initial thicknesses of Zone a and Zone b in the M-K model
e^a, e^b	Current thicknesses of Zone a and Zone b in the M-K model
f_0	Initial imperfect parameter in the M-K model (e_0^b / e_0^a)
Δt	Time increment
F_i	Newton-Raphson equation
J	Jacobian matrix
j_{ij}	Components of Jacobian matrix J
J^*	Adjoint matrix of Jacobian matrix J

$\bar{\sigma}$	Equivalent flow stress
$\bar{\varepsilon}$	Equivalent plastic strain
$\dot{\bar{\varepsilon}}$	Equivalent plastic strain rate
σ_{ij}	Stress components
ε_{ij}	Strain components
$\Delta\bar{\varepsilon}$	Equivalent plastic strain increment
$\Delta\varepsilon_{ij}$	Components of strain increment
ρ	Strain path in Zone a ($\varepsilon_{22}^a / \varepsilon_{11}^a$)
η	Stress ratio in Zone a ($\sigma_{22}^a / \sigma_{11}^a$)
γ, δ, χ, ζ	Contracted notations

$K_1^v, K_2^v, K_3^v, K_4^v, m_0^v, m_1^v$	Parameters in the modified Voce constitutive model
$K_0^l, K_1^l, n_0^l, n_1^l, m_0^l, m_1^l$	Parameters in the modified Ludwik constitutive model
$B^k, n_1^k, n_2^k, n_3^k, m^k, C_0^k, C_1^k$	Parameters in the modified KHL constitutive model
H, F, G, N, L, M	Anisotropic parameters of Hill48 yield criterion

1. Introduction

The formability of metal sheets is currently evaluated widely by the forming limit curves (FLCs) proposed by Keeler and Backofen [1]. In the theoretical methods for obtaining the FLCs, Marciniak-Kuczynski (M-K) model is the most widely used one. The M-K model was proposed by Marciniak and Kuczynski [2], in which an initial geometrical imperfection was assumed to trigger the occurrence of the localized necking, as shown in Fig.1. The imperfection is

characterized by a long groove, which may be caused by local grain size, alloy inhomogeneity or non-uniform sheet thickness distribution etc.. In the original M-K model, the initial groove is perpendicular to the principal axis-1 (Ψ_0=0), as shown in Fig. 1 (a), and it can be only applied to calculate the limit strains on the right side of FLCs. Nowadays, the M-K model has undergone great improvements, becoming one of the most important tools to predict forming limits of metal sheet.

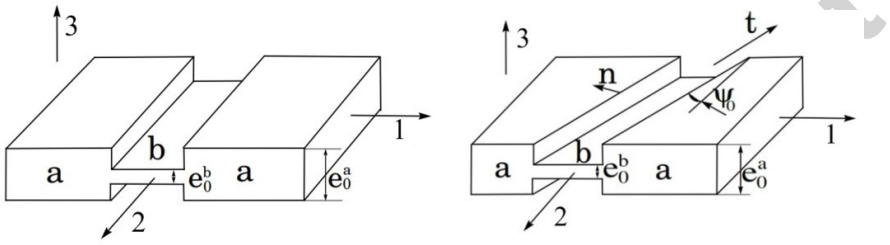

(a) Original M-K model (b) M-K model with an inclined groove

Fig. 1. Representation of the M-K model.

Using the M-K model, Sowerby and Duncan [3] analyzed the occurrence of localized necking under biaxial tension state when the minor strain was positive. Hutchinson et al. [4] extended the M-K model to negative strain paths in the case that the initial groove inclined at an angle Ψ_0 with respect to the principal axis-1 (Fig. 1 (b)). Their work showed that limit strains varied with the initial groove orientation under uniaxial tension state (noted as $\Psi_0 \neq 0$ in the following context when the limit strains are calculated by considering the variation of the initial groove angle). For anisotropic materials, Barata Da Rocha et al. [5] also found that limit strains were mostly obtained with a non-zero initial groove angle. Therefore, in the current literatures, many scholars considered the variation of the initial groove angle when the M-K model was used to obtain the left side of the FLCs, and the minimum value of the calculated limit strains with all angles was set as one point on the FLCs. But for the right side of FLCs, most scholars assumed that forming limit

was independent of the initial groove angle and the strain obtained with Ψ_0=0 was regarded as the limit strain. For example, combining the M-K model with Ψ_0=0 and Hill93 yield criterion, Banabic and Dannenmann [6] obtained the entire FLCs and analyzed the influence of the yield curve shape upon FLCs. Avila and Vieira [7] developed a code to calculate the right side of FLCs. Five different yield criteria (Von Mises, Hill48, Hill79, Hosford and Hill93 yield criterion) were implemented into M-K model and the influence of yield criterion on FLCs were investigated. The AA5083 sheet formability was investigated by Zhang et al. [8] using M-K model, Swift hardening law and Von Mises yield criterion. Both theoretical (M-K method) and numerical (Marciniak simulation test) results showed that the formability of this alloy seemed not to be improved up to a certain temperature, above this temperature, the formability was greatly enhanced. Khan and Baig [9] obtained the FLCs of AA5182-O at different temperatures (293-473K) and strain rates (10^{-4}-$1s^{-1}$) using the M-K model along with the Khan-Huang-Liang (KHL) constitutive model and Barlat's YLD96 yield criterion. Similarly, the initial groove angle with Ψ_0=0 was adopted in the work to calculate the limit strains. By comparison with other published results, their predicted results were validated. The theoretical prediction of the FLCs of aluminum-lithium 2198-T3 was obtained by Li et al. [10] based on the M-K theory with von Mises, Hill48, Hosford and Barlat 89 yield functions respectively, and the predicted FLCs with different yield functions were verified compared to the experimental ones. Using the M-K model with Ψ_0=0 and a constitutive model considering the effects of temperature and strain rate, the forming limit of Ti-6Al-4V was calculated by Li et al. [11]. The comparison with experimental results showed that the predicted FLCs under positive strain path were accurate and reliable.

In the literature, only a few scholars deduced the M-K algorithm and obtained the entire FLCs

by considering the variation of the initial groove angle, while the used constitutive laws were almost in simple forms. Butuc et al. [12] carried out the M-K analysis to obtain FLCs using a new general code. Two different constitutive models (Swift and Voce model) and four different yield criteria (Von Mises, Hill48, Hill79 and Barlat YLD96 yield criterion) were implemented into the M-K model. Their study showed that both constitutive model and yield criterion had great influences on the FLCs. A theoretical prediction and an experimental determination of the FLCs for AISI 304 stainless steel under a linear strain path were performed by Campos et al. [13]. The M-K model, Hill48 yield function and the Swift equation were used in the theoretical prediction. It was found that the experimental FLCs and the computed limit strains had a good correlation. Based on the M-K model with an inclined groove, Ganjiani and Assempour [14] developed a methodology for predicting FLCs. Two yield functions (Hosford and BBC2000) and two hardening laws (power law and Voce) were applied to predict the FLCs of AK steel and AA5XXX. Comparison with experimental data showed that for these two materials, the accuracy of the predicted results using Hosford and BBC2000 yield functions was different. Using Von Mises yield criterion and a power law function, Eyckens et al. [15] extended the M-K model to predict localized necking in sheet metal forming operations in which through-thickness shear (TTS) occurred. By introducing a new force equilibrium condition and several new compatibility conditions, the FLCs considering TTS under monotonic deformation modes were presented. Combining Hollomon hardening law with five different yield criteria (Hill48, Barlat89, Hill90, Hill93 and CPB06 yield criterion), Dasappa et al. [16] obtained FLCs of AA5754 using the M-K theory. The influence of yield surface shape, anisotropy in yield stresses and R-values were also investigated. Results showed that the yield surface shape had the most significant influence on the

FLCs using the M-K analysis with phenomenological yield functions. A numerical code based on the M-K model and a power law function was developed by Nurcheshmeh and Green [17] to predict the FLCs of sheet metals and to account for the effects of non-linear strain path and the normal stress. Their results were validated by comparing corresponding experimental FLCs at different pre-strain magnitudes and stress states. Using five power-hardening laws with different forms, Hashemi's group had done much work [18-22] on the M-K model: the through thickness compressive normal stress and strain rate were taken into account in the extended models, which lead to more accurate predictions of FLCs. What's more, a new solution for strain gradient approach of M-K method was developed. Comparison with experimental data showed that the calculated forming limit diagram (FLD) could predict the forming limit accurately, especially for the right hand side of FLD.

Aluminum alloys are very sensitive to strain rate at elevated temperatures, and their sheet formabilities are affected by both temperature and strain rate [23]. However, in current literatures, simple constitutive models were generally adopted for the deduction of M-K algorithm. The interacting effects of temperature and strain rate were well not taken into account, which lowered the accuracy of the predicted FLCs. Even though a few scholars considered the variation of the initial groove angle, there was little research about whether the initial groove angle has influence on the right side of FLCs and what the influence is. Therefore, the object of this work is to deduce the M-K algorithm for predicting the FLCs of AA5086 sheet by combining Hill48 anisotropic yield criterion and three complex constitutive models (modified Voce, Ludwik and KHL model). The influences of the initial groove angle in the M-K model on limit strains and the entire FLCs will be investigated. The comparison between predicted FLCs with the M-K model and

experimental ones by Marciniak tests under different forming conditions will also be carried out in the work.

2. Material characteristic

2.1. Uniaxial tensile test

To obtain the true stress-strain curves of AA5086 sheet, whose mechanical properties are shown in Table 1, uniaxial tensile tests under different temperatures (20, 150 and 200℃) and strain rates (0.02, 0.2 and $2s^{-1}$) are performed on a servo-hydraulic tensile machine equipped with a heating furnace. The geometry and dimensions of the tensile specimen used in this work are illustrated in Fig. 2. The specimen has the strain gauge length of 80 mm, the section width of 10 mm and thickness of 2 mm. True stress-strain curves at different forming conditions are plotted by analyzing experimental data, as shown in Fig. 3.

Table1

Mechnical properties of AA5086 sheet at ambient temperature.

Thickness (mm)	Yield strength (MPa)	Tensile strength (MPa)	Uniform elongation (%)
2	134.6	316	0.17

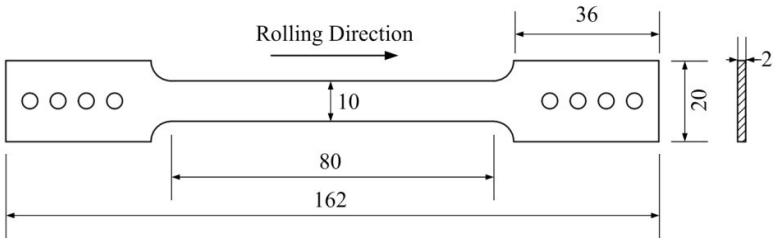

Fig. 2. Geometry and dimensions of the tensile specimen (unit: mm).

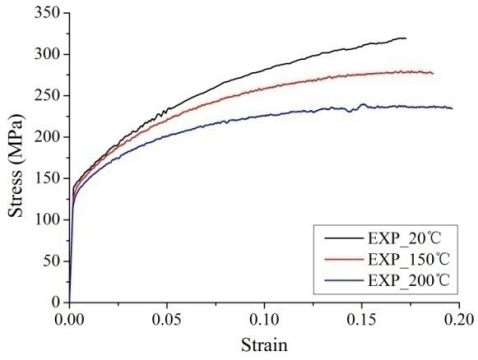

(a) $0.02s^{-1}$

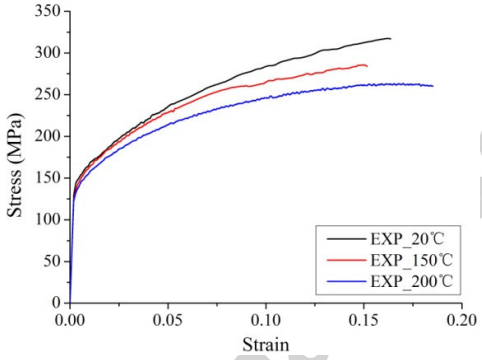

(b) $0.2s^{-1}$

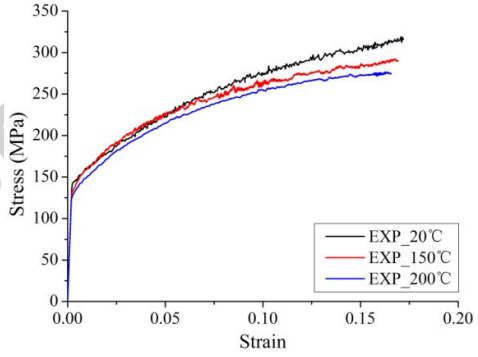

(c) $2s^{-1}$

Fig. 3. True stress-strain curves under different temperatures and strain rates.

2.2. Constitutive models

In this section, three different constitutive models (Voce, Ludwik and KHL model) are modified and material parameters of each constitutive model are obtained by the inverse analysis.

The detailed modification process and parameter identification procedure were described in the previous work of present co-author [24]. Here, only the expressions, identified material parameters and the comparison between the predicted stress-strain curves and experimental data are shown.

2.2.1. Modified Voce constitutive model

The modified Voce constitutive model is expressed as:

$$\bar{\sigma} = \sigma_0(T) + K_1^v \exp(-K_2^v T)\sqrt{1-\exp(-K_3^v \exp(K_4^v T)\bar{\varepsilon})}\,\dot{\bar{\varepsilon}}^{(m_0^v \exp(m_1^v T))} \quad (1)$$

Where, $\sigma_0(T)$ is the yield stress at a certain temperature, $\bar{\varepsilon}$ and $\dot{\bar{\varepsilon}}$ are equivalent plastic strain and equivalent plastic strain rate, respectively. $K_1^v, K_2^v, K_3^v, K_4^v, m_0^v$ and m_1^v are constant material parameters. For AA5086, the material parameters of the constitutive model are obtained by the inverse analysis, as listed in Table 2.

Table 2

Material parameters of the modified Voce constitutive model for AA5086.

K_1^v (MPa)	K_2^v (1/℃)	K_3^v	K_4^v (1/℃)	m_0^v	m_1^v (1/℃)
485.96	0.004532	0.9434	0.00903	0.00009159	0.03153

2.2.2. Modified Ludwik constitutive model

The modified Ludwik constitutive model is expressed as:

$$\bar{\sigma} = \sigma_0(T) + (K_0^l - K_1^l T)\bar{\varepsilon}^{(n_0^l - n_1^l T)}\,\dot{\bar{\varepsilon}}^{(m_0^l \exp(m_1^l T))} \quad (2)$$

Where, $K_0^l, K_1^l, n_0^l, n_1^l, m_0^l$ and m_1^l are material parameters of the modified Ludwik constitutive model, and the identified values for AA5086 are listed in Table 3.

Table 3

Material parameters of the modified Ludwik constitutive model for AA5086.

$K_0^l(MPa)$	$K_1^l(MPa/℃)$	n_0^l	$n_1^l(1/℃)$	m_0^l	$m_1^l(1/℃)$
537.41	0.9753	0.5667	0.0007207	0.00008811	0.0319

2.2.3. Modified KHL constitutive model

The modified KHL constitutive model is expressed as:

$$\bar{\sigma} = \sigma_0(T) + B^k(1-\frac{\ln\dot{\bar{\varepsilon}}}{\ln D_0})^{n_1^k}\bar{\varepsilon}^{\left(n_2^k - n_3^k T\right)}(\frac{T_m - T}{T_m - T_r})^m(\frac{\dot{\bar{\varepsilon}}}{\dot{\varepsilon}_0})^{(C_0^k \exp(C_1^k T))} \quad (3)$$

Where, T_m=627℃ is the melting temperature of AA5086, T_r=20℃ is the reference temperature, $\dot{\varepsilon}_0 = 1s^{-1}$ and D_0 is the maximum strain rate (fixed to $10^6 s^{-1}$), respectively. $B^k, n_1^k, n_2^k, n_3^k, m^k, C_0^k$ and C_1^k are material parameters of the modified KHL constitutive model. The identified values of AA5086 are listed in Table 4.

Table 4

Material parameters of the modified KHL constitutive model for AA5086.

$B^k(MPa)$	n_1^k	n_2^k	$n_3^k(1/℃)$	m^k	C_0^k	$C_1^k(1/℃)$
510.4	0.1235	0.5706	0.0007557	1.1345	0.0004105	0.02506

Fig. 4 shows the comparison of the experimental stress-strain curves and predicted ones by three constitutive models. It can be observed that in the experimental strain range (below 0.18), all three constitutive models give a good prediction of flow stress under different testing conditions. But for a high strain level (from 0.18 to 0.5), two different flow stress prediction variations are observed with different constitutive models. The predicted flow stress with Voce model shows a saturation tendency, while a monotonic increasing trend of stress vs. strain with Ludwik and KHL models is found. Coincidentally, Ludwik and KHL models give almost the same prediction of

flow stress under each forming condition.

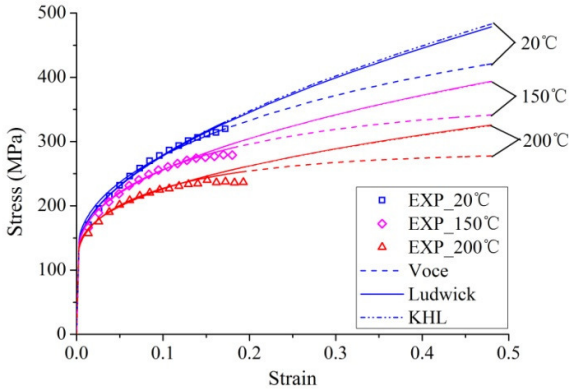

(a) $0.02s^{-1}$

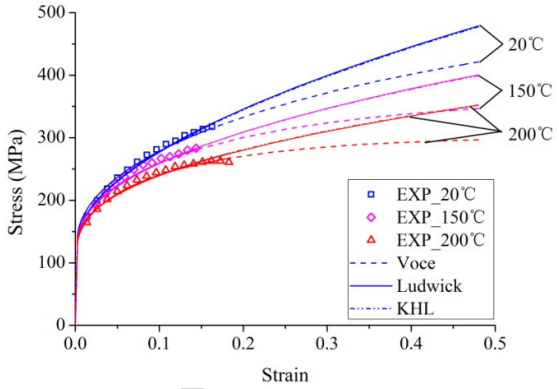

(b) $0.2s^{-1}$

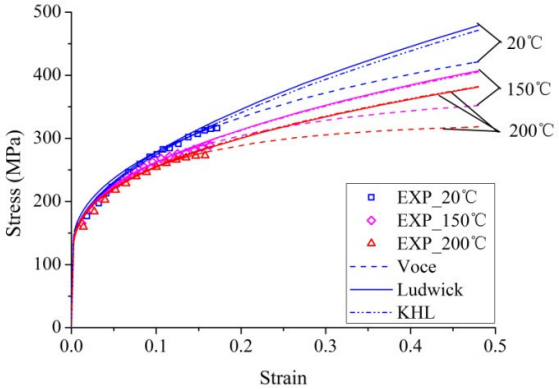

(c) $2s^{-1}$

Fig. 4. Comparison of experimental results with predicted flow stresses up to 0.5 of strain.

2.3 Yield criterion

In this paper, Hill48 yield criterion is used to describe the yield characteristic of anisotropic

materials and its general expression is [25]:

$$2\bar{\sigma}^2 = H(\sigma_{xx}-\sigma_{yy})^2 + F(\sigma_{yy}-\sigma_{zz})^2 + G(\sigma_{zz}-\sigma_{xx})^2 + 2N\sigma_{xy}^2 + 2L\sigma_{yz}^2 + 2M\sigma_{zx}^2 \quad (4)$$

Where, *x, y* and *z* are along the rolling direction, transverse direction and normal direction of the sheet, respectively. *H*, *F*, *G*, *N*, *L* and *M* are anisotropic constants of the sheet, which are determined by uniaxial tensile tests. In our previous work [26], the anisotropic parameters of AA5086 in Hill48 yield criterion have been obtained by experiment, as shown in Table 5.

Table 5

Anisotropic parameters of AA5086 sheet in Hill48 yield criterion [26].

F	*G*	*H*	*L*	*M*	*N*
0.7	0.637	0.363	1.5	1.5	1.494

3. Formula derivation and algorithm of the Marciniak-Kuczynski (M-K) model

In order to study the influence of the initial groove angle of the M-K model on forming limits, the model with the initial groove inclined at an angle Ψ_0 with respect to the principal axis-1 is taken in this paper, as shown in Fig.1 (b). The initial thickness imperfection is characterized by an initial imperfection factor f_0:

$$f_0 = \frac{e_0^b}{e_0^a} (e_0^b < e_0^a) \quad (5)$$

Where, e_0^a, e_0^b are the initial sheet thicknesses in Zone *a* and Zone *b,* respectively.

3.1. Basic hypotheses of the M-K model

In the M-K model, the sheet is assumed to be in a plane stress state ($\sigma_{13}^k = \sigma_{23}^k = \sigma_{33}^k = 0$). Then Hill48 yield criterion is reduced to:

$$2(\bar{\sigma}^k)^2 = (\sigma_{11}^k)^2(H+G) + (\sigma_{22}^k)^2(H+F) - 2H\sigma_{11}^k\sigma_{22}^k + 2N(\sigma_{12}^k)^2 \quad (6)$$

Where $\bar{\sigma}^k$ is the equivalent stress, $\sigma_{11}^k, \sigma_{12}^k$ and σ_{22}^k are stress tensor components. *k*=*a* or *b*

represents Zone *a* and Zone *b* in the M-K model, respectively.

The sheet obeys Levy-Mises's flow rule, which can be expressed as:

$$\Delta\varepsilon_{ij}^{k} = \frac{\partial\bar{\sigma}^{k}}{\partial\sigma_{ij}^{k}}\Delta\bar{\varepsilon}^{k}, \qquad i, j = 1, 2 \tag{7}$$

Where $\Delta\varepsilon_{ij}^{k}$ and $\Delta\bar{\varepsilon}^{k}$ are the increments of strain components and the equivalent plastic strain, respectively, and Δ refers to an increment corresponding to a tiny time period Δt.

Incompressibility condition is assumed during this analysis:

$$\Delta\varepsilon_{11}^{k} + \Delta\varepsilon_{22}^{k} + \Delta\varepsilon_{33}^{k} = 0 \tag{8}$$

3.2. Basic equations of the M-K model

The same force in the direction-*n* is transmitted across Zone *a* and Zone *b*. Therefore, the two zones must satisfy the force equilibrium equations, as expressed by:

$$\sigma_{nn}^{a}e^{a} = \sigma_{nn}^{b}e^{b}, \sigma_{nt}^{a}e^{a} = \sigma_{nt}^{b}e^{b} \tag{9}$$

Where e^{a}, e^{b} are the current sheet thicknesses in Zone *a* and Zone *b,* respectively.

The strain in Zone *b*, parallel to the groove (direction-*t*), is constrained by that in Zone *a,* so that compatibility condition is:

$$\Delta\varepsilon_{tt}^{a} = \Delta\varepsilon_{tt}^{b} \tag{10}$$

When a small increment of the principal strain $\Delta\varepsilon_{11}^{a}$ is imposed in Zone *a*, the groove will rotate with a corresponding angle $\Delta\Psi$. The relationship between $\Delta\varepsilon_{11}^{a}$ and $\Delta\Psi$ was expressed as Eq. (11) by Butuc et al. [12], which is also adopted in this work.

$$\tan(\Psi + \Delta\Psi) = \frac{1+\Delta\varepsilon_{11}^{a}}{1+\Delta\varepsilon_{22}^{a}}\tan\Psi \tag{11}$$

3.3. Computing process of the limit strains with the M-K algorithm

For the sake of convenience, the following simplified expressions are used:

$$\rho=\frac{\Delta\varepsilon_{22}^{a}}{\Delta\varepsilon_{11}^{a}},\eta=\frac{\sigma_{22}^{a}}{\sigma_{11}^{a}},\gamma=\frac{\sigma_{22}^{b}}{\sigma_{11}^{b}},\delta=\frac{\sigma_{12}^{b}}{\sigma_{11}^{b}} \tag{12}$$

$$\begin{cases}\chi^{a}=\sqrt{(G+H)-2H\eta+(H+F)\eta^{2}}\\ \chi^{b}=\sqrt{(G+H)-2H\gamma+(H+F)\gamma^{2}+2N\delta^{2}}\\ \zeta^{a}=\cos^{2}\Psi+\eta\sin^{2}\Psi\\ \zeta^{b}=\cos^{2}\Psi+\gamma\sin^{2}\Psi+2\delta\sin\Psi\cos\Psi\end{cases} \tag{13}$$

Using the transformation matrix, the stress and strain components in the *n-t* local coordinate system can be calculated according to the corresponding values in the global one. Combined the flow rule (Eq.(7)), the equilibrium equations (Eq.(9)) and the compatibility equation (Eq.(10)), the following non-linear equations can be obtained:

$$\begin{cases}F_{1}(\Delta\bar{\varepsilon}^{b},\gamma,\delta)=\bar{\sigma}^{a}\cdot e_{0}^{a}\cdot\chi^{b}.\zeta^{a}-\bar{\sigma}^{b}\cdot e_{0}^{b}\cdot\chi^{a}.\zeta^{b}.\exp(\varepsilon_{33}^{b}-\varepsilon_{33}^{a}+\Delta\varepsilon_{33}^{b}-\Delta\varepsilon_{33}^{a})=0\\ F_{2}(\Delta\bar{\varepsilon}^{b},\gamma,\delta)=(\eta-1)\cdot\zeta^{b}\cdot\sin\Psi\cos\Psi-\zeta^{a}\cdot\left[\delta(\cos^{2}\Psi-\sin^{2}\Psi)+(\gamma-1)\sin\Psi\cos\Psi\right]=0\\ F_{3}(\Delta\bar{\varepsilon}^{b},\gamma,\delta)=\Delta\varepsilon_{tt}^{b}\cdot\chi^{b}-\Delta\bar{\varepsilon}^{b}\left[\left[(G+H)-H\cdot\gamma\right]\sin^{2}\Psi+\left[(H+F)\gamma-H\right]\cos^{2}\Psi-4N\delta\sin\Psi\cos\Psi\right]=0\end{cases} \tag{14}$$

Where, the material's flow stress $\bar{\sigma}^{k}$ can be replaced by the three modified constitutive models (Eq.(1), Eq.(2) or Eq.(3)).

In this work, a proportional load path in Zone a is assumed, and the strain path ρ and the strain increment $\Delta\varepsilon_{11}^{a}$ in Zone *a* are imposed. The equivalent plastic strain rate $\dot{\bar{\varepsilon}}^{k}$ can be expressed as $\dot{\bar{\varepsilon}}^{k}=\Delta\bar{\varepsilon}^{k}/\Delta t$. Therefore, $\Delta\bar{\varepsilon}^{a},\eta,\Psi$ and $\Delta\varepsilon_{tt}^{b}$ in Eq.(14) can be directly calculated, resulting that only $\Delta\bar{\varepsilon}^{b},\gamma$ and δ are unknown. To solve the non-linear equations, Newton-Raphson method is used. Here, the modified Voce constitutive model and Hill48 yield criterion are taken as an example to introduce the solution procedures of the equations.

Firstly, the Jacobian matrix *J* is calculated:

$$J=\begin{pmatrix} j_{11} & j_{12} & j_{13} \\ j_{21} & j_{22} & j_{23} \\ j_{31} & j_{32} & j_{33} \end{pmatrix}=\begin{pmatrix} \dfrac{\partial F_1}{\partial \Delta\bar{\varepsilon}^b} & \dfrac{\partial F_1}{\partial \gamma} & \dfrac{\partial F_1}{\partial \delta} \\ \dfrac{\partial F_2}{\partial \Delta\bar{\varepsilon}^b} & \dfrac{\partial F_2}{\partial \gamma} & \dfrac{\partial F_2}{\partial \delta} \\ \dfrac{\partial F_3}{\partial \Delta\bar{\varepsilon}^b} & \dfrac{\partial F_3}{\partial \gamma} & \dfrac{\partial F_3}{\partial \delta} \end{pmatrix} \tag{15}$$

The components of the Jacobian matrix are obtained as follows:

$$\begin{aligned} j_{11}=\frac{\partial F_1}{\partial \Delta\bar{\varepsilon}^b}=-\frac{e_0^b}{e_0^a}\exp(\varepsilon_{33}^b-\varepsilon_{33}^a+\Delta\varepsilon_{33}^b-\Delta\varepsilon_{33}^a)\cdot\chi^a\cdot\zeta^b\cdot\Bigg(&\frac{K_1^v\exp(-K_2^vT)}{2\sqrt{1-\exp(-K_3^v\exp(K_4^vT)(\bar{\varepsilon}^b+\Delta\bar{\varepsilon}^b)}}\cdot \\ &\exp(-K_3^v\exp(K_4^vT))(\bar{\varepsilon}^b+\Delta\bar{\varepsilon}^b)K_3^v\exp(K_4^vT)\cdot\left(\frac{\Delta\bar{\varepsilon}^b}{\Delta t}\right)^{m_0^v\exp(m_1^vT)}+ \\ &K_1^v\exp(-K_2^vT)\sqrt{1-\exp(-K_3^v\exp(K_4^vT)(\bar{\varepsilon}^b+\Delta\bar{\varepsilon}^b)}\cdot m_0^v\exp(m_1^vT)\cdot\frac{1}{\Delta t}\cdot\left(\frac{\Delta\bar{\varepsilon}^b}{\Delta t}\right)^{m_0^v\exp(m_1^vT)-1}\Bigg) \end{aligned} \tag{16-1}$$

$$j_{12}=\frac{\partial F_1}{\partial \gamma}=\frac{\bar{\sigma}^a\cdot\zeta^a\cdot((H+F)\gamma-H)}{\chi^b}-\chi^a\cdot\frac{e_0^b}{e_0^a}\exp(\varepsilon_{33}^b-\varepsilon_{33}^a+\Delta\varepsilon_{33}^b-\Delta\varepsilon_{33}^a)\cdot\sin^2\Psi\cdot\bar{\sigma}^b \tag{16-2}$$

$$\begin{aligned} j_{13}=\frac{\partial F_1}{\partial \delta}=&\frac{2\cdot N\cdot\delta\cdot\zeta^a\cdot\bar{\sigma}^a}{\chi^b}- \\ &2\cdot\frac{e_0^b}{e_0^a}\exp(\varepsilon_{33}^b-\varepsilon_{33}^a+\Delta\varepsilon_{33}^b-\Delta\varepsilon_{33}^a)\cdot\bar{\sigma}^b\cdot\chi^a\cdot\sin^2\Psi\cdot\cos^2\Psi \end{aligned} \tag{16-3}$$

$$j_{21}=\frac{\partial F_2}{\partial \Delta\bar{\varepsilon}^b}=0 \tag{16-4}$$

$$j_{22}=\frac{\partial F_2}{\partial \gamma}=(\eta-1)\cdot\sin^3\Psi\cdot\cos\Psi-\zeta^a\cdot\sin\Psi\cdot\cos\Psi \tag{16-5}$$

$$j_{23}=\frac{\partial F_2}{\partial \delta}=2\cdot(\eta-1)\cdot\sin^2\Psi\cdot\cos^2\Psi-\zeta^a\cdot(\cos^2\Psi-\sin^2\Psi) \tag{16-6}$$

$$j_{31}=\frac{\partial F_3}{\partial \Delta\bar{\varepsilon}^b}=-\Big[\big[(G+H)-H\gamma\big]\sin^2\Psi+\big[(H+F)\gamma-H\big]\cos^2\Psi-4N\delta\sin\Psi\cos\Psi\Big] \tag{16-7}$$

$$j_{32}=\frac{\partial F_3}{\partial \gamma}=\frac{(H+F)\gamma-H}{\chi^b}\Delta\varepsilon_{tt}^a-\Delta\bar{\varepsilon}^b((H+F)\cos^2\Psi-H\sin^2\Psi) \tag{16-8}$$

$$j_{33}=\frac{\partial F_3}{\partial \delta}=\frac{2N\delta\Delta\varepsilon_{tt}^a}{\chi^b}+4N\sin\Psi\cos\Psi\Delta\bar{\varepsilon}^b \tag{16-9}$$

The iterative process of Newton-Raphson method is:

$$\begin{pmatrix} \Delta\bar{\varepsilon}^{b(i+1)} \\ \gamma^{(i+1)} \\ \delta^{(i+1)} \end{pmatrix}=\begin{pmatrix} \Delta\bar{\varepsilon}^{b(i)} \\ \gamma^{(i)} \\ \delta^{(i)} \end{pmatrix}-J^{-1}\cdot\begin{pmatrix} F_1(\Delta\bar{\varepsilon}^{b(i)},\gamma^{(i)},\delta^{(i)}) \\ F_2(\Delta\bar{\varepsilon}^{b(i)},\gamma^{(i)},\delta^{(i)}) \\ F_3(\Delta\bar{\varepsilon}^{b(i)},\gamma^{(i)},\delta^{(i)}) \end{pmatrix}=\begin{pmatrix} \Delta\bar{\varepsilon}^{b(i)} \\ \gamma^{(i)} \\ \delta^{(i)} \end{pmatrix}-\frac{J^*}{|J|}\cdot\begin{pmatrix} F_1(\Delta\bar{\varepsilon}^{b(i)},\gamma^{(i)},\delta^{(i)}) \\ F_2(\Delta\bar{\varepsilon}^{b(i)},\gamma^{(i)},\delta^{(i)}) \\ F_3(\Delta\bar{\varepsilon}^{b(i)},\gamma^{(i)},\delta^{(i)}) \end{pmatrix} \tag{17}$$

Where J^* is the adjoint one of the Jacobian matrix *J*.

The iterative process begins after the initial values of $\Delta\bar{\varepsilon}^b, \gamma$ and δ are given, and ends with the satisfaction of the necking criterion ($\Delta\bar{\varepsilon}^b/\Delta\bar{\varepsilon}^a \geq 7$). The corresponding major and minor strains (ε_{11}^a and ε_{22}^a) are identified as the limit strains for a certain initial groove angle. The computational process is repeated for different values of Ψ_0 (between 0 and $\pi/2$) and only the minimum limit strains can be used to draw the FLCs. The flow chart for the whole computing process is shown in Fig. 5.

(1) Set the initial imperfection parameter f_0, the forming temperature *T*, the strain rate $\dot{\bar{\varepsilon}}^a$ and impose a strain increment $\Delta\varepsilon_{11}^a$ along the direction-1 in Zone *a*.

(2) Give a strain path ρ and compute $\eta, \Delta\bar{\varepsilon}^a$ and $\Delta T = \Delta\bar{\varepsilon}^a/\dot{\bar{\varepsilon}}^a$.

(3) Set initial groove angle Ψ_0, compute the current groove angle Ψ, and the values of χ^a, χ^b, ζ^a and ζ^b.

(4) Solve the equations (14) by Newton-Raphson method to get $\Delta\bar{\varepsilon}^b, \gamma$ and δ.

(5) Update $\varepsilon_{11}^a, \varepsilon_{22}^a$ and compute $\Delta\bar{\varepsilon}^b/\Delta\bar{\varepsilon}^a$ to check whether the local necking occurs.

(6) If the necking criterion is not satisfied, then update the current groove angle Ψ and repeat Step 4 and Step 5 until $\Delta\bar{\varepsilon}^b/\Delta\bar{\varepsilon}^a \geq 7$.

(7) When the necking criterion is satisfied, a group of limit strains for a certain initial groove angle are obtained.

(8) Check whether the initial groove angle Ψ_0 is less than $\pi/2$. Updating Ψ_0 and return back to Step 3 if the above condition is satisfied. Otherwise, go to the next step.

(9) Compare limit strains obtained at different initial groove angles under a given strain path and choose the minimum one as the limit point on FLCs.

(10) Check whether the strain path ρ is less than 1. If it is true, return back to Step 2. Otherwise, stop the whole computational process.

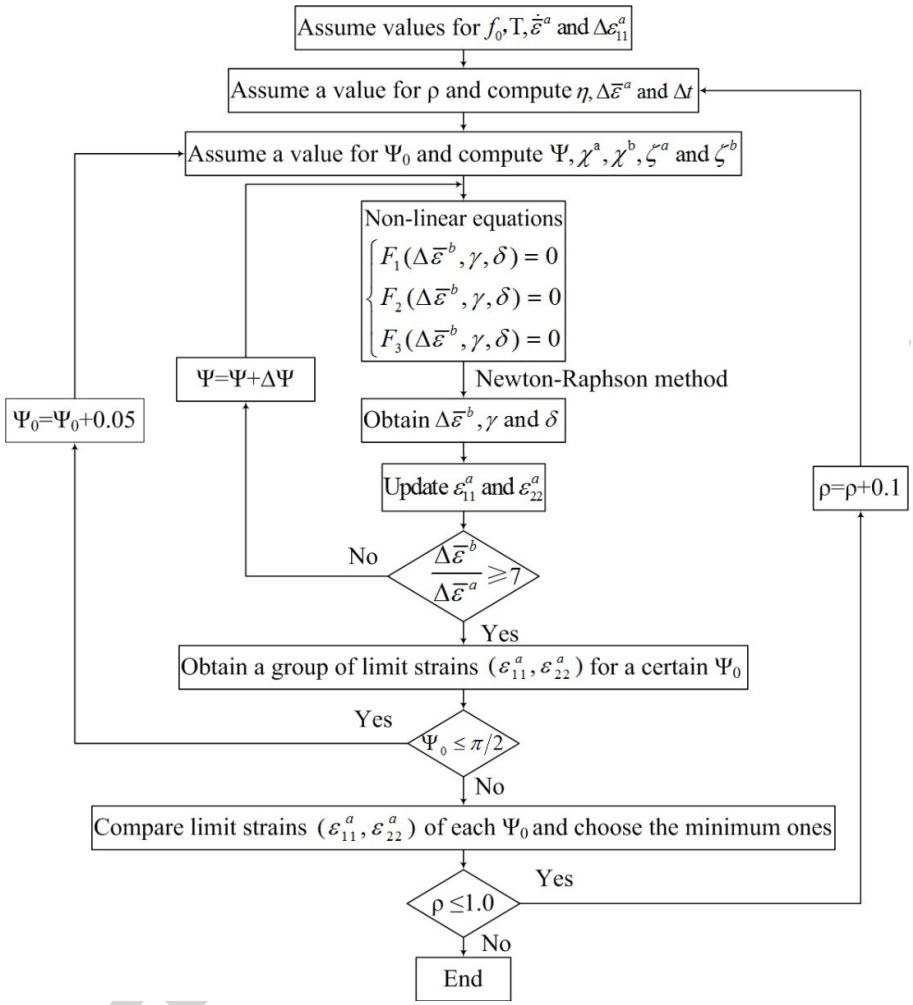

Fig. 5. Flow chart of computing process of FLCs with the M-K model.

4. Results discussion based on the M-K model

4.1. Influence of the necking criterion on the FLCs

According to the equilibrium equations (Eq.(9)) and the compatibility condition (Eq.(10)), the strain ε_{11}^b is always larger than that in Zone a. Here, taking the modified Voce constitutive model as an example, two strain paths in Zone a ($\rho^a=-0.4$ and $\rho^a=1.0$) are chosen to illustrate the evolution process of strain increments in Zone *a* and Zone *b*, as shown in Fig. 6. It can be seen

that the strain path is always constant in Zone *a*, while in Zone *b* it evolves stably until a certain moment, after which it increases abruptly. At this moment, the plastic deformation is localized, and the deformation condition in the groove moves towards a 'relative plane strain condition' $(\Delta\varepsilon_{22}^{b}/\Delta\varepsilon_{11}^{b}=0)$, while the corresponding ratio of strain increments in Zone *a* remains constant. This is the necessary condition for the occurrence of the localized necking.

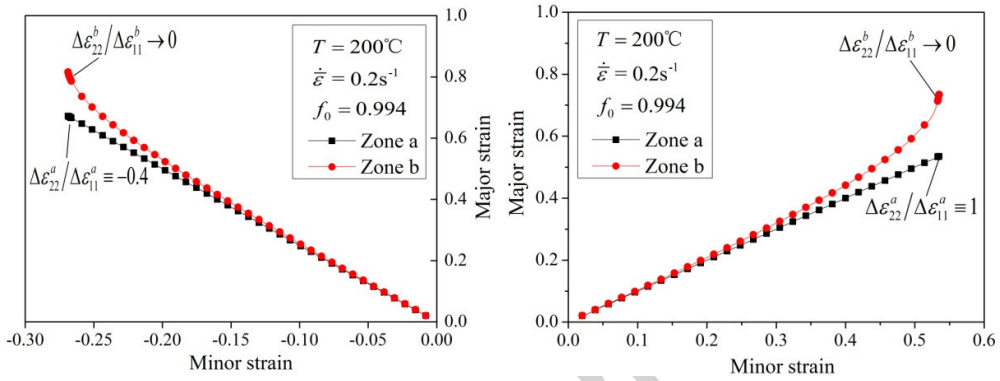

(a) ρ=-0.4 (b) ρ=1.0

Fig. 6. Evolution of strain paths inside and outside the groove for ρ=-0.4 and ρ=1.0.

The necking criterion in the M-K model was defined in different ways. In the work of Marciniak and Kuczynski [2], the necking was considered to occur when the imperfection factor (e^{b}/e^{a}) dropped below a critical value. Barata Da Rocha et al. [5] put forward that the necking happened when the ratio ($\Delta\bar{\varepsilon}^{b}/\Delta\bar{\varepsilon}^{a}$) was greater than 10 while Banabic et al. [27] assumed that this critical value was 7. To evaluate the influence of necking criterion on the determination of FLCs, various values of $\Delta\bar{\varepsilon}^{b}/\Delta\bar{\varepsilon}^{a}$ are chosen in this work, as shown in Fig. 7. From this figure, there is no significant difference between FLCs determined by $\Delta\bar{\varepsilon}^{b}/\Delta\bar{\varepsilon}^{a}\geq 7$, $\Delta\bar{\varepsilon}^{b}/\Delta\bar{\varepsilon}^{a}\geq 10$ and $\Delta\bar{\varepsilon}^{b}/\Delta\bar{\varepsilon}^{a}\geq 15$. This can also be explained by the strain evolutions from Fig. 6. During the deformation process, the plastic strain in Zone *b* will rapidly increase after a certain moment, leading to a rapid change of $\Delta\bar{\varepsilon}^{b}/\Delta\bar{\varepsilon}^{a}$ in a small time increment, while major and minor strains

in Zone a keeps almost constant. Therefore, even if the value of $\Delta\bar{\varepsilon}^b/\Delta\bar{\varepsilon}^a$ changes a lot, there is no clear influence on the level of FLCs. Hence, $\Delta\bar{\varepsilon}^b/\Delta\bar{\varepsilon}^a \geq 7$ is reasonable as a necking criterion for stopping the above numerical iteration.

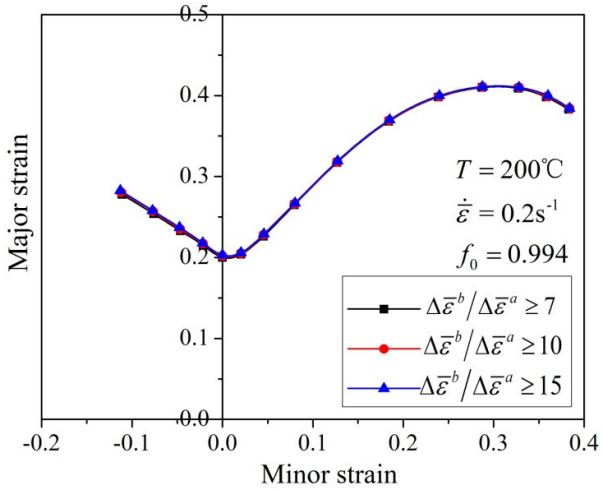

Fig. 7. Comparison of FLCs obtained with different necking criteria.

4.2. Influence of the initial groove angle on limit strains and FLCs

The influence of the initial groove angle in the M-K model on limit major strains is investigated with the algorithm developed in this work, as shown in Fig. 8, which is calculated with the modified Voce constitutive model and Hill48 yield function.

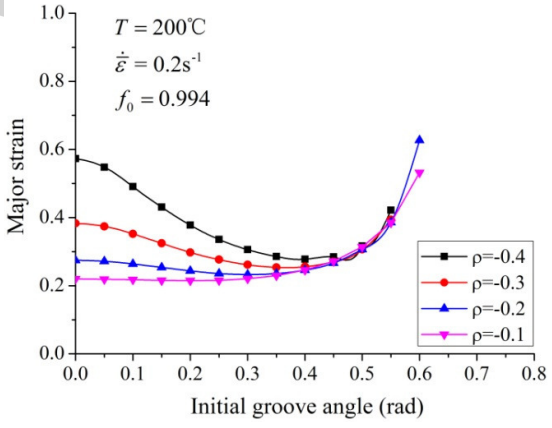

(a) -0.4 ≤ρ≤ -0.1

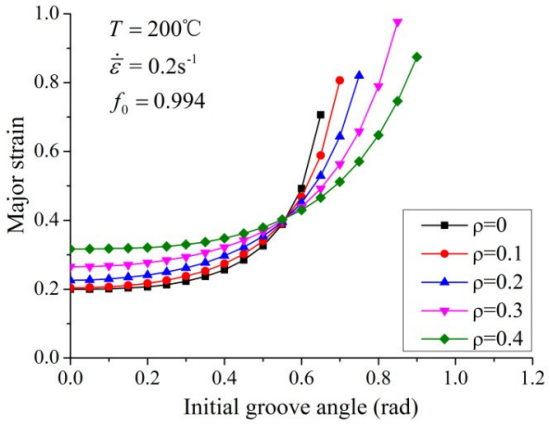

(b) 0 ≤ρ≤ 0.4

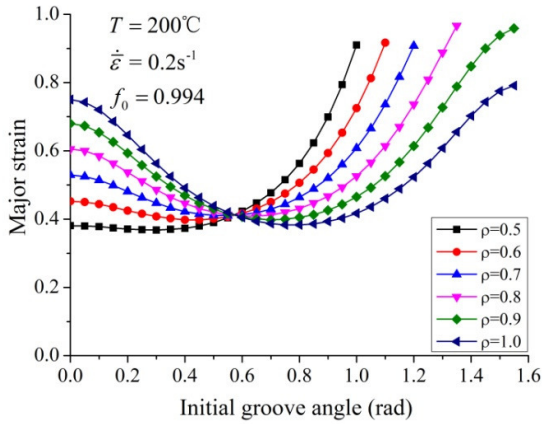

(c) 0.5 ≤ρ≤ 1

Fig. 8. Influences of the initial groove angle in the M-K model on limit major strains under different strain paths (with the Modified Voce constitutive model and Hill48 yield criterion).

It can be observed from Fig. 8 that the initial groove angle has great influence on limit major strains under different strain paths, and accordingly the entire strain path range is divided into three parts.

For the left side of FLCs (Fig. 8(a), ρ<0), with the increasing initial groove angle, limit major strain decreases at first and then increases, and this tendency becomes much more obvious when the deformation condition is close to uniaxial tensile state. Thus, FLCs are sensitive to the initial groove angle under negative strain paths. To accurately determine the FLCs, varying initial groove

angles in the M-K model should be considered, which is consistent with the treating approaches and conclusions in the literatures.

But for the right side of FLCs, when the strain path is in the range between 0 to 0.4, the limit major strain shows a monotonic increase with the rising initial groove angle and the minimum limit major strain is always obtained with Ψ_0=0.

However, when strain path is in the range from 0.5 to 1.0, the dependence of limit major strain on initial groove angle shows a similar tendency to that in the left side of FLCs. With the increasing initial groove angle, limit major strain decreases at first and then increases, and this tendency becomes more obvious when strain path is close to 1.0. Therefore, according to the above analysis, for a strain path in the range from 0.5 to 1.0, the sheet formability in literatures obtained by assuming initial groove angle equal to zero overestimates clearly its true sheet formability.

Moreover, an interesting phenomenon can be observed from Fig. 8: for the right side of FLCs, the evolution curves of major strains in terms of the initial groove angle always intersect at one point with the initial groove angle of about 0.55 rad. That is to say, when the initial groove angle in the M-K model is near 0.55 rad (about 31.51°), limit major strains are independent of strain paths, and the nearly equal value of limit major strains are obtained under different strain paths (from 0 to 1.0). On the other hand, for the left side of FLC, a similar intersecting point is also observed at the initial groove angle of about 0.55 rad. Therefore, when the initial groove angle in the M-K model is 0.55 rad, FLCs obtained by this model is nearly a straight line, especially for the right side of FLCs, as shown in Fig. 9.

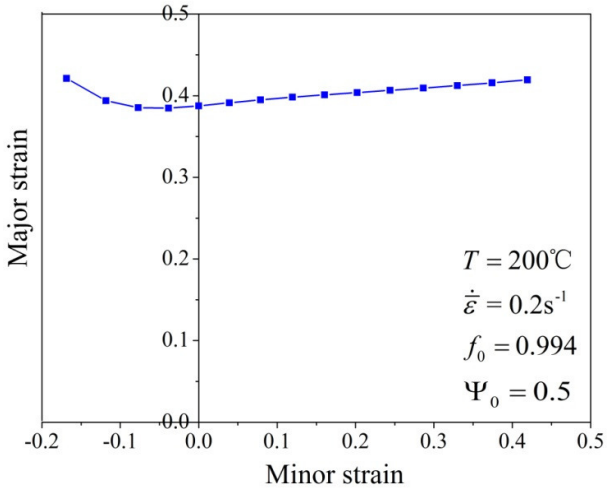

Fig. 9. Limit strains obtained with Ψ_0=0.55 rad in the M-K model.

Additionally, the modified Ludwik and KHL constitutive models are also implemented into the M-K model to investigate the influence of the initial groove angle on critical limit strains. The similar influencing tendency is found to that obtained with the modified Voce constitutive model. The only difference is that the intersection points in Fig. 8 vary with different constitutive models.

Therefore, when using the M-K model to calculate the forming limits, the influence of the initial groove angle must be taken into account for the left side of FLCs and for a strain path between 0.5 and 1.0. In this case, forming limits obtained with $\Psi_0 \neq 0$ are less than that obtained with Ψ_0=0, and limit strain should be achieved at a certain initial groove angle between 0 and $\pi/2$. While the strain path is in the range from 0 to 0.4, forming limits are achieved with Ψ_0=0. Fig. 10 shows the FLCs obtained with different constitutive models. The variation of the initial groove angle is always taken into account for the left side of FLCs. To compare the influence of the initial groove angle on FLCs, two cases with Ψ_0=0 and $\Psi_0 \neq 0$ are considered for the right side of FLCs, respectively.

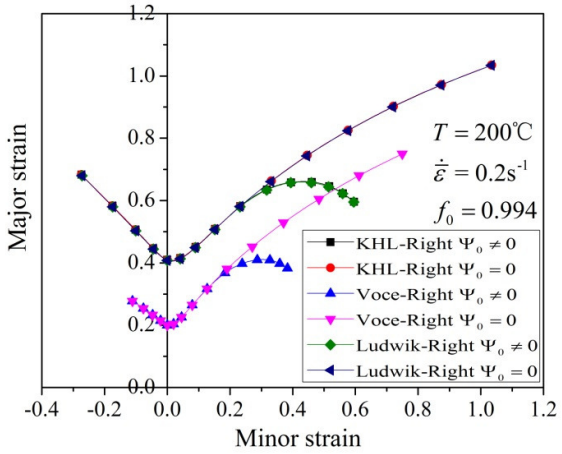

Fig. 10. FLCs obtained using different constitutive models.

From this figure, FLCs obtained using three different constitutive models show similar shape in both cases with Ψ_0=0 and Ψ_0≠0. With same forming conditions and imperfection factor, the modified Ludwik and KHL models give a higher prediction of FLCs compared to the Modified Voce model. Combining with Fig. 4, it is found that the modified Voce model shows a saturated prediction of flow stress, while the Ludwik and KHL models always give a monotonic increasing flow stress. Therefore, it is concluded that the power law-based hardening model (Ludwik and KHL model) generates higher predictions of sheet formability, which is most probably caused by the non-saturated hardening. The identical observations were also seen in several literatures. Aghaie-Khafri and Mahmudi [28] found that for AA3105-H and AA8011, FLCs predicted by the power law-equation was higher than that by the Voce model. For AA3003-H111, Abedrabbo et al. [29] pointed out that the Voce hardening law predicted lower FLCs than that by the power law.

4.3. Influence of yield criterion on FLCs

In this section, the modified Voce constitutive model will be used as an example to investigate the influence of yield criterion on FLCs, as shown in Fig. 11.

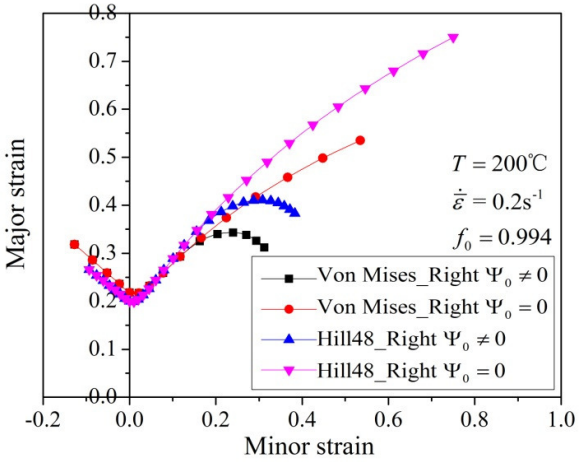

Fig. 11. Influence of yield criterion on FLCs.

The FLCs with similar shapes are observed using Von Mises and Hill 48 yield criterion (The anisotropic parameters are list in Table 5.), but the levels of FLCs are different. For the left side of FLCs (ρ<0), forming limits are not sensitive to yield criterion. But for the right side of FLCs (ρ>0), the yield criterion has a great influence on FLCs, especially when strain path is close to 1.0 (biaxial tension state). The forming limits obtained with Hill48 yield criterion are much higher than that with Von Mises yield criterion. The similar conclusion is also found in the work of Butuc et al. [12], in which the M-K model was used to study the influence of yield criterion on FLCs of AA6016.

5. Execution of Marciniak tests and verification of the developed algorithm

In this section, Marciniak tests under different strain rates (0.02, 0.2 and $2s^{-1}$) and temperatures (20, 150 and 200℃) are carried out to experimentally obtain FLCs of AA5086. The experimental setup is shown in Fig. 12. To cover a large range of strain paths as possible, 13 specimens with different shapes are tested, and the digital image correlation (DIC) technique is used to analyze the deformation evolution and to measure the strains of the specimens.

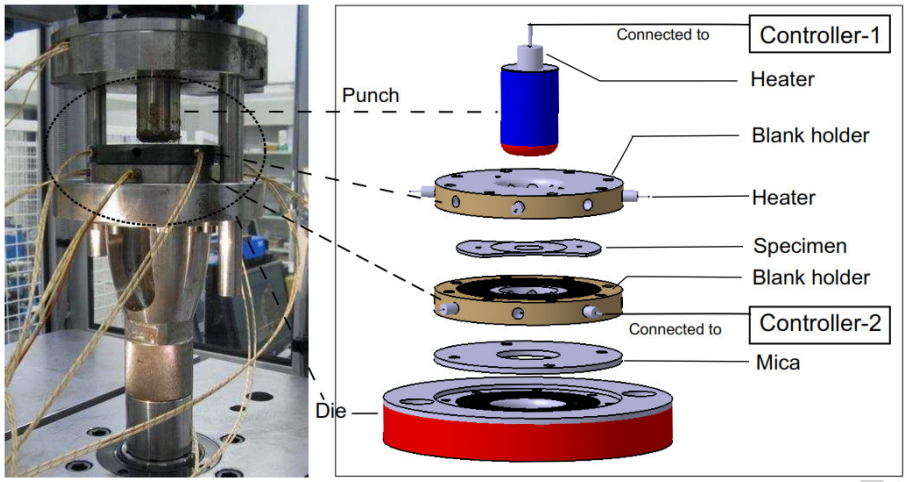

Fig. 12. The Marciniak setup.

FLCs of AA5086 obtained under different forming conditions are shown in Fig. 13. Taking into account of the insensitivity of AA5086 to strain rate at ambient temperature, only Marciniak test of $2s^{-1}$ is performed at 20℃, in which the experimental data will be taken as references for other strain rates at room temperature.

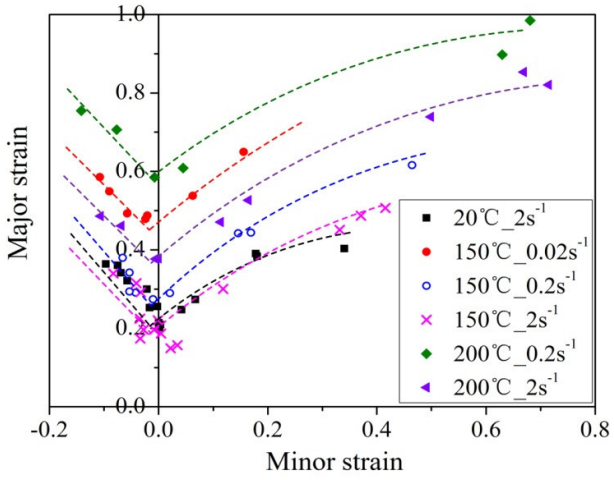

Fig. 13. FLCs of AA5086 with the Marciniak test at different temperatures and strain rates.

From the figure, both temperature and strain rate have significant influences on forming limits. The positive effect of temperature and the negative effect of strain rate on the forming limit can be clearly observed. For a given strain rate, the FLC_0 (the value of major strain under plane strain

state) increases obviously with increasing temperatures except that the whole FLCs at 20 and 150 ℃ are very close when the strain rate is $2s^{-1}$. On the contrary, the FLC_0 decreases with increasing strain rate at a given temperature. At 150℃, when the strain rate reduces from $2s^{-1}$ to $0.2s^{-1}$ and $0.02s^{-1}$, the order of the FLC_0 increment is 35% and 92%, respectively. In addition, due to the interacting effects of temperature and strain rate, the positive effect of temperature on sheet formability may be offset by the negative effect of strain rate. For example, the FLCs at 150℃ and $0.02s^{-1}$ is a little higher than that at 200℃ and $2s^{-1}$.

To compare with experimental results, three different constitutive models and Hill48 yield function are implemented into the M-K model to theoretically obtain FLCs. The right side of FLCs obtained with $\Psi_0=0$ and $\Psi_0\neq0$ are both considered. Under each forming condition, the initial imperfection factor f_0 in the M-K model will be adjusted to fit well with the experimental ones. Due to the limitation of the algorithm developed in this paper, forming limits at 20℃ cannot be calculated with KHL constitutive model. As a result, only the calculated results at 150 and 200℃ are compared with experimental ones. The comparisons of predicted and experimental results are shown in Fig. 14-16.

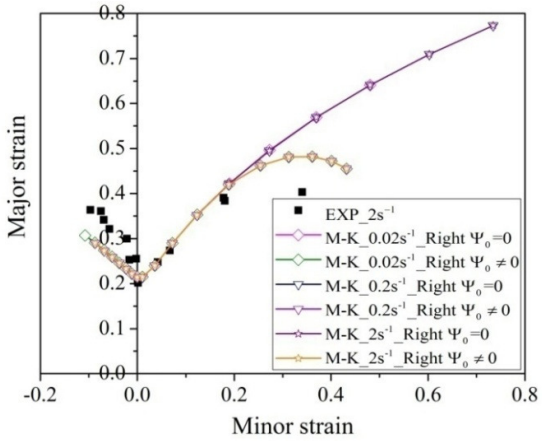

(a) 20℃

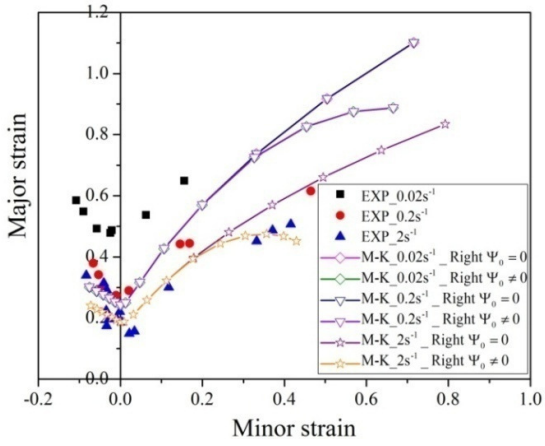

(b) 150℃

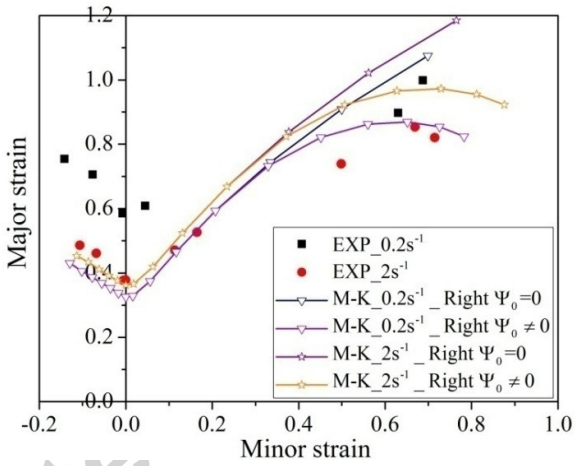

(c) 200℃

Fig. 14. Comparison of experimental data and FLCs calculated with modified Voce constitutive model and Hilll48 yield criterion.

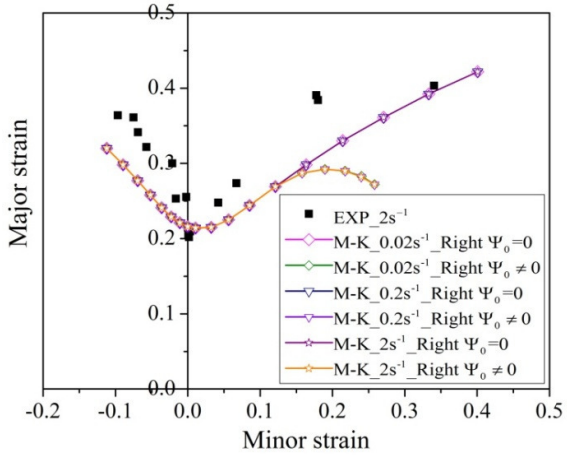

(a) 20℃

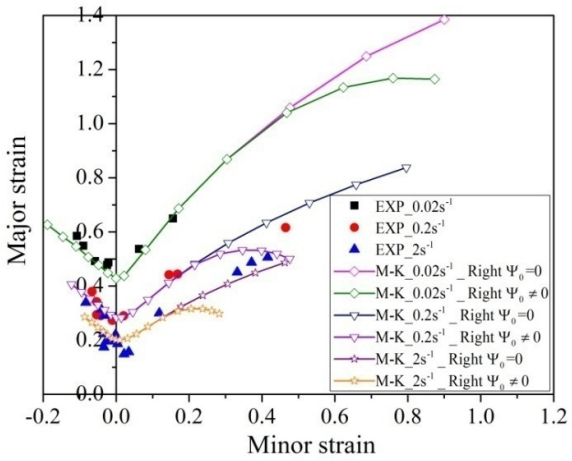

(b) 150℃

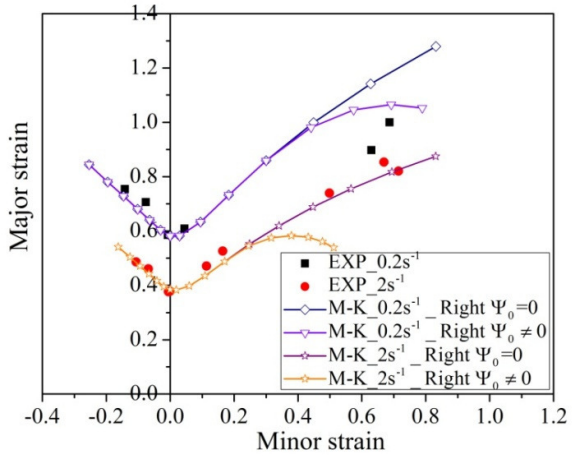

(c) 200℃

Fig. 15. Comparison of experimental data and FLCs calculated with modified Ludwik constitutive model and Hilll48 yield criterion.

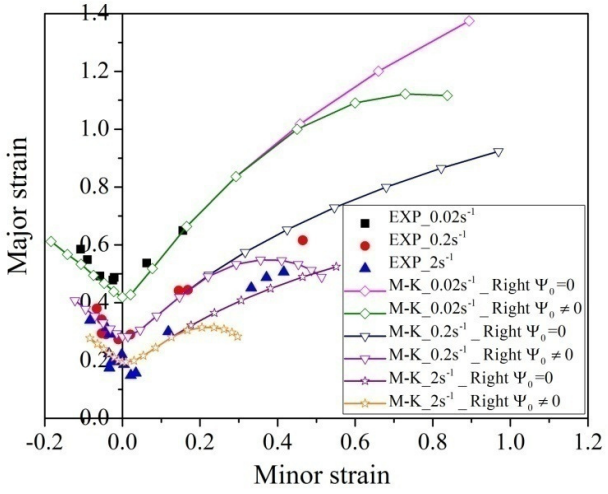

(a) 150℃

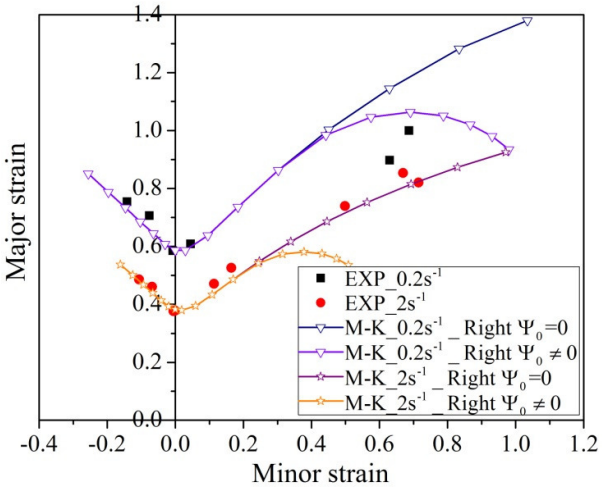

(b) 200℃

Fig. 16. Comparison of experimental data and FLCs calculated with modified KHL constitutive model and Hilll48 yield criterion.

It can be concluded from Figs. 14-16 that in the ranges of temperature and strain rate covered in this work, the predicted FLCs with modified Ludwik and KHL constitutive models are generally in good agreement with experimental results, especially at left side of FLCs. The maximum errors are 10.34% and 12.43% under plane strain state (at 150℃and $0.02s^{-1}$) for two constitutive models, respectively. Compared to the predicted FLCs with modified Ludwik and KHL constitutive models, there is great discrepancy between the predicted FLCs with the modified Voce model and experimental ones, especially at 150℃and $0.02s^{-1}$ or at 200℃and $0.2s^{-1}$, and the errors arrive at 51.31% and 44.27% under plane strain condition, respectively. The saturation of the modified Voce constitutive model affects the evolution of strain and stress around the necking localization[30], which is probably the reason that the modified Voce constitutive model underestimates the experimental FLCs at 150℃and $0.02s^{-1}$ or at 200℃and $0.2s^{-1}$.

A further observation shows that, at high temperature for example as shown in Fig.16 (b), when the strain path is greater than 0.5 and the strain rate is relatively low ($0.2s^{-1}$), the predicted

FLCs with $\Psi_0 \neq 0$ agree better with experimental data than those with $\Psi_0=0$. But for higher strain rates ($2s^{-1}$), when the strain path is greater than 0.5, the predicted FLCs with $\Psi_0 \neq 0$ do not show better matches with experimental ones than those with $\Psi_0=0$. And when the strain ratio is low, both cases show little discrepancy which consistent with the conclusion in Section 4 that no limit strain difference between the cases with $\Psi_0 \neq 0$ and $\Psi_0=0$ is found when the strain path is within 0.4. Taking into account that material parameters in all constitutive models are identified with only low strain levels (below 0.18), the use of material parameters identified with low strains may lead to inaccurate or uncertain prediction of FLCs at high strains.

In order to further verify the algorithm and conclusions obtained in this work, in the following future, material parameters will be identified by more enough experimental data (e.g. hot compression test). And also, more Marciniak tests will be performed to cover a larger strain path range.

6. Conclusions

In this work, the M-K algorithm is developed by combining Hill48 anisotropic yield criterion and three complex constitutive models. The influence of the initial groove angle of the M-K model on limit strains and FLCs are investigated. The conclusions are drawn as follows:

(1) Under different strain paths, the initial groove angle has markedly different influence on limit major strains. When the strain path is less than 0 or greater than 0.5, limit strain depends greatly on the initial groove angle of the M-K model. In this case, the various initial groove angles must be taken into account when calculating FLCs. However, in most current literatures, the influence of the initial groove angle is ignored, resulting that the calculated FLCs overestimates clearly its true sheet formability. When the strain path is between 0 and 0.4, the minimum limit

strain obtained with a zero initial groove angle. In this case, when calculating FLCs, the variation of initial groove angle could be neglected.

(2) When the initial groove angle in the M-K model is near 0.55 rad (about 31.51°), limit major strains are independent of strain path. Limit major strains under different strain paths are approximately the same and the FLCs calculated at this angle is almost a straight line.

(3) The constitutive model has great influence on the determination of FLCs by the M-K algorithm developed in this work. With same forming conditions and imperfection factor, the modified Ludwick and KHL models give a higher prediction of FLCs compared to the Modified Voce model. By comparison with experimental FLCs obtained by the Marciniak test, the modified Ludwik and KHL constitutive models give a good prediction for FLCs of AA5086 while there is great discrepancy between experimental and predicted results with the modified Voce constitutive model.

Acknowledgements

The authors would like to acknowledge financial support from National Natural Science Foundation of China (51105230 and 51405266), and Natural Science Foundation of Shandong Province(ZR2014EEP003)

References:

[1] Keeler, SP, Backofen, WA. Plastic instability and fracture in sheets stretched over rigid punches. Asm. Trans. Q. 1963;56; 25-48.

[2] Marciniak Z, Kuczyński K. Limit strains in the processes of stretch-forming sheet metal. Int. J. Mech. Sci. 1967;9:609-20.

[3] Sowerby R, Duncan JL. Failure in sheet metal in biaxial tension. Int. J. Mech. Sci.

1971;13:217-29.

[4] Hutchinson JW, Neale KW, Needleman A. Mechanics of sheet metal forming. Plenum Press, New York. 1978.

[5] Barata Da Rocha A, Barlat F, Jalinier JM. Prediction of the forming limit diagrams of anisotropic sheets in linear and non-linear loading. Mater. Sci. Eng. 1985;68:151-64.

[6] Banabic D, Dannenmann E. Prediction of the influence of yield locus on the limit strains in sheet metals. J. Mater. Process. Tech. 2001;109:9-12.

[7] Avila AF, Vieira E. Proposing a better forming limit diagram prediction: a comparative study. J. Mater. Process. Tech. 2003;141:101-8.

[8] Zhang C, Leotoing L, Guines D, Ragneau E. Theoretical and numerical study of strain rate influence on AA5083 formability. J. Mater. Process. Tech. 2009;209:3849-58.

[9] Khan AS, Baig M. Anisotropic responses, constitutive modeling and the effects of strain-rate and temperature on the formability of an aluminum alloy. Int. J. Plast. 2011;27:522-38.

[10] Li X, Song N, Guo G, Sun Z. Prediction of forming limit curve (FLC) for Al-Li alloy 2198-T3 sheet using different yield functions. Chin. J. Aeronaut. 2013;26:1317-23.

[11] Li X, Guo G, Xiao J, Song N, Li D. Constitutive modeling and the effects of strain-rate and temperature on the formability of Ti-6Al-4V alloy sheet. Mater. Des. 2014;55:325-34.

[12] Butuc MC, Gracio JJ, Da Rocha AB. A theoretical study on forming limit diagrams prediction. J. Mater. Process. Tech. 2003;142:714-24.

[13] Campos HB, Butuc MC, Grácio JJ, Rocha JE, Duarte JMF. Theorical and experimental determination of the forming limit diagram for the AISI 304 stainless steel. J. Mater. Process. Tech. 2006;179:56-60.

[14] Ganjiani M, Assempour A. An improved analytical approach for determination of forming limit diagrams considering the effects of yield functions. J. Mater. Process. Tech. 2007;182:598-607.

[15] Eyckens P, Van Bael A, Van Houtte P. Marciniak-Kuczynski type modelling of the effect of through-thickness shear on the forming limits of sheet metal. Int. J. Plast. 2009;25:2249-68.

[16] Dasappa P, Inal K, Mishra R. The effects of anisotropic yield functions and their material parameters on prediction of forming limit diagrams. Int. J. Solids. Struct. 2012;49:3528-50.

[17] Nurcheshmeh M, Green DE. The effect of normal stress on the formability of sheet metals under non-proportional loading. Int. J. Mech. Sci. 2014;82:131-9.

[18] Assempour A, Safikhani AR, Hashemi R. An improved strain gradient approach for determination of deformation localization and forming limit diagrams. J. Mater. Process. Tech. 2009;209:1758-69.

[19] Safikhani AR, Hashemi R, Assempour A. Some numerical aspects of necking solution in prediction of sheet metal forming limits by strain gradient plasticity. Mater. Des. 2009;30:727-40.

[20] Hashemi R, Ghazanfari A, Abrinia K, Assempour A. The effect of the imposed boundary rate on the formability of strain rate sensitive sheets using the MK method. J. Mater. Eng. Perform. 2013;22:2522-7.

[21] Hashemi R, Abrinia K, Assempour A, Nejadkhaki HK, Mastanabad AS. Forming limit diagram of tubular hydroformed parts considering the through-thickness compressive normal stress. Proc. IMechE. Part L. J. Mater. Des. Appl. 2014; 1464420714562652.

[22] Hashemi R, Mamusi H, Masoumi A. A simulation-based approach to the determination of

forming limit diagrams. Proceedings of the Institution of Mechanical Engineers, Part B: Journal of Engineering Manufacture. 2014;0954405414522448.

[23] Tarigopula V, Hopperstad OS, Langseth M, Clausen AH, Hild F. A study of localisation in dual-phase high-strength steels under dynamic loading using digital image correlation and FE analysis. Int. J. Solids. Struct. 2008;45:601-19.

[24] Chu XR. Caractérisation expérimentale et prédiction de la formabilité d'un alliage d'aluminium en fonction de la température et de la vitesse de déformation[D]. INSA de Rennes.2013.

[25] Hill R. A theory of the yielding and plastic flow of anisotropic metals. Proceedings of the Royal Society of London. Series A. Math. Phys. Sci. 1948;193:281-97.

[26] Leotoing L, Guines D, Zidane I, Ragneau E. Cruciform shape benefits for experimental and numerical evaluation of sheet metal formability. J. Mater. Process. Tech. 2013;213:856-63.

[27] Banabic D, Comsa S, Jurco P, Cosovici G, Paraianu L, Julean D. FLD theoretical model using a new anisotropic yield criterion. J. Mater. Process. Tech. 2004;157:23-7.

[28] Aghaie-Khafri M, Mahmudi R. Predicting of plastic instability and forming limit diagrams. Int. J. Mech. Sci. 2004;46:1289-306.

[29] Abedrabbo N, Pourboghrat F, Carsley J. Forming of aluminum alloys at elevated temperatures-Part 2: Numerical modeling and experimental verification. Int. J. Plasticity. 2006;22:342-73.

[30] Da Rocha AB, Santos AD, Teixeira P, Butuc MC. Analysis of plastic flow localization under strain paths changes and its coupling with finite element simulation in sheet metal forming. J. Mater. Process. Tech. 2009;209:5097-109.